# Kinetic Trajectory Decoding Using Motor Cortical Ensembles

Andrew H. Fagg, *Member, IEEE*, Gregory W. Ojakangas, Lee E. Miller, and Nicholas G. Hatsopoulos

***Abstract*—Although most brain–machine interface (BMI) studies have focused on decoding kinematic parameters of motion such as hand position and velocity, it is known that motor cortical activity also correlates with kinetic signals, including active hand force and joint torque. Here, we attempted to reconstruct torque trajectories of the shoulder and elbow joints from the activity of simultaneously recorded units in primary motor cortex (MI) as monkeys (*Macaca Mulatta*) made reaching movements in the horizontal plane. Using a linear filter decoding approach that considers the history of neuronal activity up to one second in the past, we found torque reconstruction performance nearly equal to that of Cartesian hand position and velocity, despite the considerably greater bandwidth of the torque signals. Moreover, the addition of delayed position and velocity feedback to the torque decoder substantially improved the torque reconstructions, suggesting that simple limb-state feedback may be useful to optimize BMI performance. These results may be relevant for BMI applications that require controlling devices with inherent, physical dynamics or applying forces to the environment.**

***Index Terms*—Multi-electrode recording, primary motor cortex, torque decoding.**

## I. Introduction

THE early pioneering electrophysiological experiments of Evarts suggested that single pyramidal tract MI neurons encode primarily the force (or its temporal derivative) applied by the limb rather than movement *per se* [1]. A dichotomy is often drawn between this early work, and that of Georgopoulos, who showed a striking relation between MI discharge and the direction of hand movement [2]. Numerous subsequent studies have provided evidence that MI encodes a variety of kinetic and kinematic signals, including joint torque and hand force [3]–[9], position [10], [11], velocity [12], direction of hand movement [2], [13]. Nonetheless, virtually all real-time brain–machine interfaces (BMIs) have focused only on kinematic variables [14]–[17].

Manuscript received July 22, 2008; revised May 08, 2009; accepted June 07, 2009. First published August 07, 2009; current version published November 04, 2009. This work was supported by National Institute of Neurological Disorders and Stroke under Grant NS048845.

A. H. Fagg is with the School of Computer Science, University of Oklahoma, Norman, OK 73019 USA (e-mail: fagg@cs.ou.edu).

G. Ojakangas is with the Department of Physics, Drury University, Springfield, M0 65802 USA (e-mail: gojakang@drury.edu).

L. E. Miller is with the Department of Physiology, Northwestern University, Chicago, IL 6061 USA (e-mail: lm@northwestern.edu).

N. G. Hatsopoulos is with the Department of Organismal Biology and Anatomy and Committee on Computational Neuroscience, University of Chicago, Chicago, IL 60637 USA (e-mail: nicho@uchicago.edu).

Color versions of one or more of the figures in this paper are available online at http://ieeexplore.ieee.org.

Digital Object Identifier 10.1109/TNSRE.2009.2029313

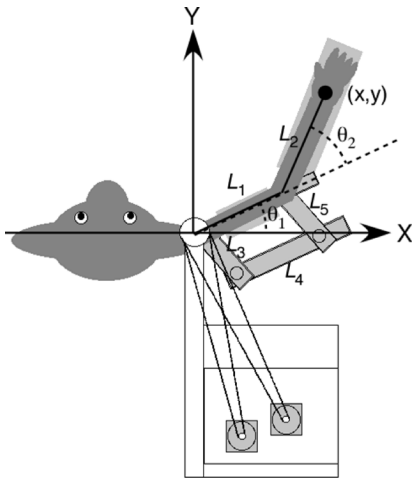


Fig. 1. Monkey's arm configuration on the exoskeletal robot (KINARM). Joint angular positions, $\theta_1$ and $\theta_2$, were sampled directly. Cartesian position of the hand $(X, Y)$ was calculated using the joint angles and arm segment lengths, $L_1$ and $L_2$.

However, an early pioneering study predicted wrist joint torque from a small number of motor cortical units [18]. More recently, a study demonstrated grip force decoded from motor cortical ensembles [19]. Moreover, EMG activity can be reconstructed from groups of MI neurons [20]–[23]. These recent decoding results, as well as the earlier force encoding studies, suggest that it should be possible to control a dynamical limb by predicting the torques generated by the shoulder and elbow joints during reaching.

We recorded simultaneously from multiple single units in MI using chronically implanted electrode arrays while monkeys performed a random-target pursuit task. This task generated a rich variety of trajectories with varied curvatures, velocities, and positions. We used linear regression techniques to predict shoulder and elbow torque from the activity of the recorded neurons, which we compared to the corresponding kinematic predictions.

## II. Methods

### A. Behavioral Tasks and Kinematics

Three monkeys (Macaca Mulatta) were used in these experiments. Each monkey's upper arm was abducted 90° and rested on cushioned troughs secured to links of a two-joint robotic arm (KINARM system; Fig. 1) [24]. The robotic arm constrained movement to a horizontal plane, but did not limit movement within this plane. The cursor and a sequence of targets were projected on a horizontal screen immediately above the monkey's arm. At the beginning of a trial, a target appeared at a random

TABLE I
DATA SET SIZES

| Data Set | Number of Cells | Average Fold Length (min) |
|---|---|---|
| RJ1 | 48 | 1.10 |
| RJ2 | 61 | 1.07 |
| BO1 | 36 | 2.32 |
| BO2 | 31 | 1.36 |
| RS1 | 99 | 1.21 |
| RS2 | 86 | 2.56 |

location in the workspace and the monkey was required to move to it. As soon as the cursor reached the target, the target disappeared and was replaced by a new one in a random location. After reaching the seventh target, the monkey was rewarded with a drop of water. The monkeys typically executed 400–800 successful trials in the course of a 1–1.5 h recording session.

The shoulder and elbow joint angles were sampled at 500 Hz using the robotic arm's motor encoders and acquired along with neural data. The $X$ and $Y$ positions of the hand were computed by transforming the joint angles into Cartesian endpoints using the standard forward kinematics equations for a two-joint arm [25]. The lengths of the upper arm and forearm of the monkey were estimated using X-ray images of the humerus and the distance from the elbow joint to the palm, respectively.

### B. Electrophysiology

Silicon-based electrode arrays (Blackrock Microsystems, Inc., Salt Lake City, UT) composed of 100 electrodes (1.0 mm electrode length; 400 $\mu$m inter-electrode separation) were implanted in the arm area of primary motor cortex (MI) contralateral to the moving arm on the precentral gyrus of each monkey. Surgical implantation was performed using Isoflurane. During a recording session, signals from up to 96 electrodes were amplified (gain, 5000) and digitized (14-bit) at 30 kHz per channel using a Cerebus acquisition system (Blackrock Microsystems, Inc.). Waveforms that crossed a threshold were stored and spike-sorted using Offline Sorter (Plexon, Inc., Dallas, TX). Inter-spike interval histograms were computed to verify single-unit isolation by ensuring that less than 0.05% of waveforms possessed an inter-spike interval less than 1.6 ms. Signal-to-noise ratios (SNRs) were defined as the difference in mean peak-to-trough voltage of the waveforms divided by the mean (over all 48 time samples of the waveform) standard deviation of the waveforms. All isolated single units used in this study possessed SNRs of 4:1 or higher. Two data sets were analyzed from each of three animals, BO, RJ, and RS (see Table I). A data set is defined as all simultaneously recorded neural and kinematic data collected in one recording session. Each data set contained between 31 and 99 simultaneously recorded units from MI. The ensembles consisted of "randomly" selected units from MI except for a possible bias for neurons with large cell bodies that would generate higher SNRs. All of the surgical and behavioral procedures were approved by the University of Chicago's IACUC and conform to the principles outlined in the Guide for the Care and Use of Laboratory Animals (NIH publication no. 86-23, revised 1985).

### C. Equations of Motion

The KINARM exoskeletal robot is composed of five segments, labeled $\mathrm{L}_1$ through $\mathrm{L}_5$ in Fig. 1. As illustrated, the monkey's shoulder and elbow joints are coincident with the proximal pivot axes of segments 1 and 2. Segments 1 and 4 remain parallel at all times, as do segments 3 and 5. Segment 5 is rigidly attached to segment 2 at an angle of 155°. Torque motors 1 and 2, not actively employed in this study, are attached by belts to segments 1 and 3, and thus contribute passively to rotational inertias. Relevant arm segment inertias for the monkeys were added to those of KINARM segments 1 and 2 (with which they were coincident during valid trials). The arm segment inertias were estimated using the approach of Cheng and Scott [26] and were based on each monkey's body mass on the day the data set was recorded (see Table II and Appendix A for details). The equations of motion for the combined system consisting of the monkey's arm and the associated moving components of the KINARM were derived in a standard manner using Hamilton's principle applied to the Lagrangian for the system [27]. Expressed in terms of the planar shoulder and elbow angles $\theta_1$ and $\theta_2$ (see Fig. 1), the equations are as follows:

$$\tau_1 = A(\theta_2)\ddot{\theta}_1 + B(\theta_2)\ddot{\theta}_2 - C(\theta_2)(2\dot{\theta}_1\dot{\theta}_2 + \dot{\theta}_2{}^2) \quad (1a)$$

and

$$\tau_2 = B(\theta_2)\ddot{\theta}_1 + D\ddot{\theta}_2 + C(\theta_2)\dot{\theta}_1{}^2 \quad (1b)$$

where

$$A(\theta_2) = \sum_{i=1}^{5} I_i + I_{m1} + I_{m2} + M_2L_1^2 + M_4L_3^2 + 2g(\theta_2) \quad (2a)$$

$$B(\theta_2) = D + g(\theta_2) \quad (2b)$$

$$C(\theta_2) = M_2L_1(\overline{x_2}\sin\theta_2 + \overline{y_2}\cos\theta_2) + M_4L_3(\overline{x_4}\sin(\theta_2 - \Delta) - \overline{y_4}\cos(\theta_2 - \Delta)) \quad (2c)$$

$$g(\theta_2) = M_2L_1(\overline{x_2}\cos\theta_2 - \overline{y_2}\sin\theta_2) + M_4L_3(\overline{x_4}\cos(\theta_2 - \Delta) + \overline{y_4}\sin(\theta_2 - \Delta)) \quad (2d)$$

and

$$D = I_2 + I_3 + I_5 + I_{m2} + M_4L_3^2. \quad (2e)$$

In the above equations, $\tau_1$ and $\tau_2$ represent the net torque applied to the shoulder and elbow in order to account for the observed motion. The torques are due not only to actively generated muscle forces, but also to other viscoelastic effects that result from the musculoskeletal system, and to the KINARM. $I_i$, $M_i$, and $L_i$ are the rotational inertias (with respect to the proximal pivots), masses, and inter-joint lengths of the numbered segments, $(\overline{x}_i, \overline{y}_i)$ is the center-of-mass location of the $i$th segment in a right-handed, proximal-pivot-centered coordinate system with the $x$-axis directed along the length of the segment,

TABLE II
KINARM AND MONKEY MECHANICAL PROPERTIES

| Term | Definition | RJ1,RJ2 | B1,B2 | RS1,RS2 |
|---|---|---|---|---|
| $M_1$ | Total mass of segment 1 (g): $M_{1K}$+ $M_{1A}$ | 919 | 947 | 1390 |
| $M_2$ | Total mass of segment 2 (g): $M_{2K}$+ $M_{2A}$ | 636 | 656 | 801 |
| $M_{1K}$ | Mass of KINARM segment 1[a] (g) | 635 | 635 | 1040. |
| $M_{2K}$ | Mass of KINARM segments 2+5[a](g) | 391 | 391 | 509 |
| $M_{1A}$ | Upper arm mass of animal[b](g) | 284 | 312 | 350. |
| $M_{2A}$ | Forearm mass of animal[b](includes hand) (g) | 244 | 265 | 292. |
| $M_3$ | Mass of KINARM segment 3(g) | 637 | 637 | 978. |
| $M_4$ | Mass of KINARM segment 4(g) | 117 | 117 | 162. |
| $M_{hand}$ | Hand mass of animal[b](g) | 56 | 59 | 62. |
| $M_{forearm}$ | Forearm mass of animal[b] (excludes hand) (g) | 188 | 206 | 230. |
| $M_A$ | Total animal mass (kg) | 7.6 | 8.4 | 9.50 |
| $I_{1K}$ | Rotational inertia of KINARM segment 1[c]($gcm^2$) | $2.64x10^4$ | $2.64x10^4$ | $4.30x10^4$ |
| $I_{2K} + I_{5K}$ | Rotational inertia of KINARM segment 2+5[c]($gcm^2$) | $4.39x10^4$ | $4.66x10^4$ | $5.49x10^4$ |
| $I_{1A}$ | Rotational inertia of animal upper arm[d]($gcm^2$) | $4.51x10^4$ | $5.72x10^4$ | $4.68x10^4$ |
| $I_{2A}$ | Rotational inertia of animal forearm[d]($gcm^2$) | $3.48x10^4$ | $4.31x10^4$ | $3.47x10^4$ |
| $I_1$ | Total rotational inertia of segment 1 | | $I_{1K} + I_{1A}$ | |
| $I_2$ | Total rotational inertia of segment 2 | | $I_{2K} + I_{2A}$ | |
| $I_3$ | Rotational inertia of KINARM segment 3[c]($gcm^2$) | $1.84x10^4$ | $1.84x10^4$ | $6.38x10^4$ |
| $I_4$ | Rotational inertia of segment 4 [c] ($gcm^2$) | $1.76x10^4$ | $1.76x10^4$ | $9.00x10^3$ |
| $I_{M1}$, $I_{M2}$ | Rotational inertias of torque motors ($gcm^2$) | 7920. | 7920. | 7920. |
| $L_1$ | Length of segment #1 and monkey upper arm (cm)[e] | 13.9 | 15.0 | 13.0 |
| $L_2$ | Length of segment #2 and monkey forearm (to palm of hand, cm)[e] | 20.4 | 22.0 | 19.0 |
| $L_3$ | Inter-joint length (cm) | 6.7 | 6.7 | 6.7 |
| $l_{radius}$ | Animal radius bone length [e] (cm) | 15.5 | 17.2 | 14.3 |
| $\bar{X}_{1K}, \bar{Y}_{1K}$ | Center of mass coordinates of KINARM segment 1 (cm). | 3.24,-0.83 | 3.24,-0.83 | 2.22,-3.44 |
| $\bar{X}_{2K}, \bar{Y}_{2K}$ | Center of mass coordinate of KINARM segment 2 (cm). | 2.75,-0.83 | 2.75,-0.83 | 0.49,-1.31 |
| $\bar{X}_{3K}, \bar{Y}_{3K}$ | Center of mass coordinate of KINARM segment 3 (cm). | 3.31, 0 | 3.31, 0 | 5.52, 0 |
| $\bar{X}_{4K}, \bar{Y}_{4K}$ | Center of mass coordinate of KINARM segment 4 (cm). | 10.06, 0 | 10.06, 0 | 4.65, 0 |
| $\bar{X}_{1A}, \bar{Y}_{1A}$ | Center of mass coordinates of monkey upper arm[f](cm) | 6.95, 0 | 7.50, 0 | 6.5, 0 |
| $\bar{X}_{2A}, \bar{Y}_{2A}$ | Center of mass coordinates of monkey forearm[g](cm) | 9.93, 0 | 10.83, 0 | 8.98, 0 |

(a) $M_{1k}$ includes arm rest, and $M_{2k}$ includes forearm rest, forearm trough, and handle-grip.
(b) Masses $M_{1A}$ , $M_{2A}$ , $M_{hand}$ , $M_{forearm}$ were computed from the linear regressions described by Cheng and Scott (2000) (Table 8) based on total animal mass $M_A$.
(c) KINARM segment inertias were obtained from Ian Brown (personal communication) and subsequently modified for rotation about proximal pivots, rather than centers of mass, using the parallel axis theorem. This requires the use of the $\bar{X}_{i\,K}, \bar{Y}_{i\,K}$ values given in the Table. Inertias of arm troughs, rests, and KINARM handle were added to give total inertias of segments 1 and 2.
(d) Animal arm inertias were calculated from the regression formulae of Cheng and Scott (2000), modified for rotation about proximal pivots, rather than centers of mass.
(e) Lengths of upper arm, forearm (to palm of hand), and radius were determined from x-ray images of each monkey.
(f) Upper arm was treated as a uniform circular cylinder.
(g) Forearm center of mass (without hand) was assumed to be $0.44 \times l_{radius}$ (Cheng & Scott, 2000). Hand was treated as a point mass at position of palm (distance $L_2$ from elbow joint).

and $I_{Mi}$ are the effective rotational inertias for the shoulder- and elbow-torque motors.

### *D. Spectral Content and Filtering of Signals*

Because the differentiation required to estimate angular velocity and acceleration significantly amplifies high frequency noise, the position signals were digitally low-pass filtered below 6 Hz with a three-pole Butterworth filter. The filter was applied in both the forward and reverse directions to eliminate phase distortions [28], resulting in a composite six-pole filter. As anticipated, there remained significantly more movement-related power at frequencies above 0.5 Hz in the torque signals than in the position signals. The performance of the torque predictions was dependent on the degree of filtering: predictions improved

as the filter corner was decreased from 20 to 4 Hz. Presumably this was the result of the elimination of higher frequency differentiation noise in the torque signals. A corresponding decrease did not occur for the position predictions, as there was very little power in the original signals above several hertz. As the filter corner approached 4 Hz, there would also have been some impact on movement-related ($< 5$ Hz) frequencies. Although the ideal corner frequency for filtering remains unclear, we chose 6 Hz for the remainder of the analysis.

One form of torque decoder that we explored makes use of joint position and velocity as additional inputs to the decoder. Under these conditions, position was smoothed with a realizable (causal) 1 pole, 6-Hz Butterworth filter prior to differentiation. In practice, this filter induced an approximate delay of 50 ms in the position and velocity signals.

### *E. Analysis*

Reconstructions of Cartesian endpoint position and velocity, and shoulder and elbow torque were computed from the neural data using separate linear models. Predictions at time index $j$ (denoted $\hat{p}_j$), were obtained from the linear weighted discharge of multiple neurons at multiple time points in the past (this is referred to as a linear filter decoder or a Wiener filter) [14], [15], [19], [29]

$$\hat{p}_j = f_0 + \sum_{n=1}^{N} \sum_{i=1}^{L} r_{j-i}^{n} f_i^n \tag{3}$$

where $N$ is the number of simultaneously recorded neurons, $L$ is the filter length in number of time bins, $r_j^n$ is the discharge of neuron $n$ at time index $j$, and the $f_i^n$ denote the set of filter coefficients. The discharge of an individual neuron at one time point was estimated using the number of spikes evoked within a time bin of length $B$. $N$ ranged from 31 to 99 neurons (depending upon the data set). Following Hatsopoulos *et al.* [30], $L$ was set to 20, and $B$ was set to 50 ms, resulting in a filter length of 1 s. The values of the linear filter coefficients were selected so as to minimize the sum squared difference between the predicted quantities, $\hat{p}_j$, and the actual quantities, $p_j$, using a Moore–Penrose pseudo-inverse method [29], [31].

The performance of a given model was assessed using a test data set that was sampled independently of the data used to construct the model. Because we wish to compare prediction performance for variables of different units, we chose a unitless performance metric. A common choice for such a metric is the so-called $R^2$ statistic [16]. In the literature, this term is used to refer to both Coefficient of Determination (CoD, the square of Pearson's Correlation Coefficient) [19], [20], [32] and to the fraction of variance accounted for (FVAF) [29]. Both forms are summarized as follows:

$$R^2 = 1 - \frac{\sum_{j=1}^{M} \left(p_j - (\alpha \hat{p}_j + \beta)\right)^2}{\sum_{j=1}^{M} (p_j - \bar{p})^2} \tag{4}$$

where $M$ is the number of samples in the data set, and $\bar{p}$ is the mean over the actual quantities (for the test set). For CoD, $\alpha$ and $\beta$ are selected so as to maximize the measure, which is equivalent to minimizing the mean squared error of a linear model that predicts $p_j$ from $\hat{p}_j$. The range of this statistic is [0, 1]. For FVAF, the parameters are selected without knowledge of the test data set: $\alpha = 1$ and $\beta = 0$. The range of this statistic is $[-\infty, 1]$. FVAF is a stricter metric in that it requires a perfect match between the prediction ($\hat{p}_j$) and the observation ($p_j$), rather than a simple correlation. Because our ultimate goal is to use these predictions to drive the motion of a prosthetic or robotic arm, we chose to measure model performance using FVAF. Note that when the prediction $\hat{p}_j$ is made using a linear model (as is our case), FVAF is equal to CoD for the training data set. Hence, we interpret FVAF measures in the range [0, 1] in the same way as one would interpret CoD. We interpret negative FVAF measures as the model injecting more variance into the process than there exists in the data set.

Each model was assessed using a $K$-fold cross-validation approach (where $K = 20$ for our experiments). Here, the data set was partitioned into 20 independent "folds" [33]–[35], each consisting of data from an equal number of trials. For each fold, a separate model was constructed, leaving that fold out for use as *test data* and using eighteen of the remaining folds as training data. The test data fold was used to compare the performance across different model forms. The one remaining fold was used under certain conditions as a *validation data set*: model performance with respect to this data set was used to select some model parameters (e.g., proprioceptive feedback delay), before evaluating the model for comparison with other model forms using the test data. This approach eliminates any bias that may be introduced by selecting the model parameters on the basis of the test set performance [34].

Our choice of $K = 20$ folds in contrast to the typical choice of $K = 10$ was motivated by two factors. First, in preliminary experiments, our smallest data sets showed tendencies toward model over-fitting; the additional 10% of training data provided a margin of safety in this regard. However, further increases of $K$ result in diminishing returns. Second, the 20 FVAF measures provided a larger sample with which to perform hypotheses testing as we compared the different types of models.

In practice, the FVAF measures from a set of $N$ models were not always distributed normally. This property precludes the use of a Student's t-test for detecting significant differences in mean model performance across different types of model. We detected violations of normality using a Shapiro–Wilk test [36]. When the distribution was not normal, bootstrap sampling methods were used to estimate the sampling distribution: the shift method was used for paired tests, and randomization was performed for two-sample tests [37]. Mean model performance was then compared with these empirically-derived sampling distributions to estimate the probability of incorrectly rejecting the null hypothesis that there was no difference in performance.

### *F. Adding Proprioception Feedback to Torque Prediction*

For some of the torque predictions, the linear filter decoder model of (3) was modified to include as inputs not only the neural discharge, but also the angular positions and velocities at a delay of $\Delta$ time steps

$$\hat{\tau}_j = f_0 + f_{\dot{\theta}_1} \dot{\theta}_{1,j-\Delta} + f_{\dot{\theta}_2} \dot{\theta}_{2,j-\Delta} + f_{\theta_1} \theta_{1,j-\Delta} + f_{\theta_2} \theta_{2,j-\Delta} + \sum_{n=1}^{N} \sum_{i=1}^{L} r_{j-i}^{n} f_i^n \tag{5}$$

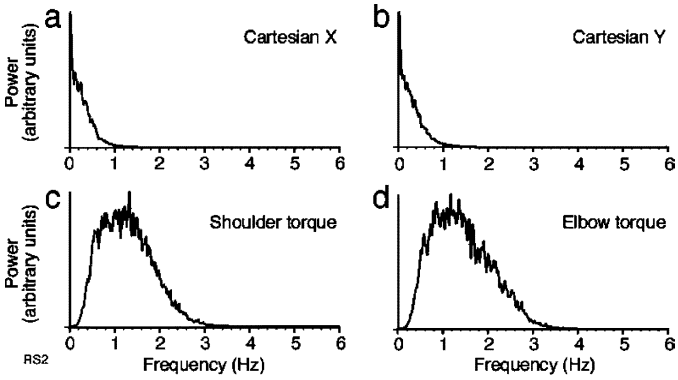


Fig. 2. Typical power spectra on linear scale plots for Cartesian X position of the hand (a), Cartesian Y position (b), shoulder joint torque (c), and elbow joint torque (d). All spectra were calculated following the 6 Hz, 6-pole filtering described in the text.

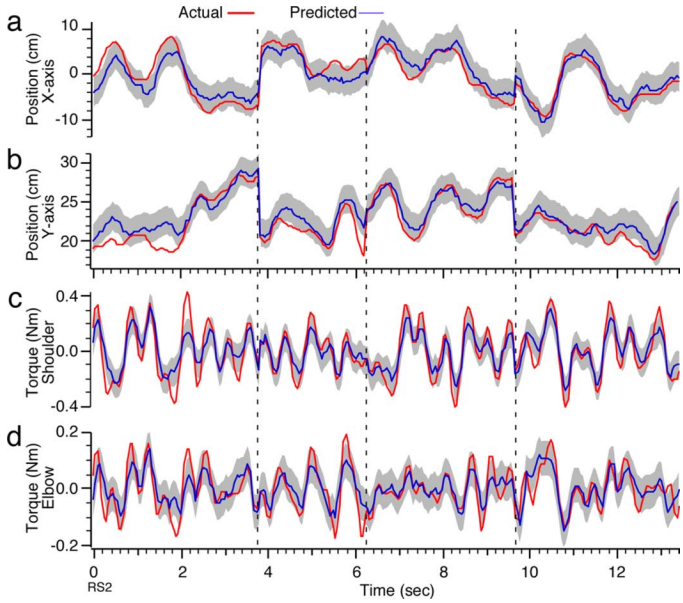


Fig. 3. Decoding of Cartesian position [(a) and (b)] and joint torque [(c) and (d)]. Thick red lines indicate actual position or torque, while the thin blue lines indicate the predicted signals estimated from the model. The gray areas represent the 95% *prediction interval* for each quantity. The dashed vertical lines represent trial boundaries.

where $\theta_{1,j-\Delta}$ and $\theta_{2,j-\Delta}$ are the shoulder and elbow joint positions sampled at the time corresponding to bin $j-\Delta$. For simplicity of modeling, both the position and velocity terms are assumed to contribute linearly to the estimate of torque. Note that the joint position and velocity signals were filtered using a casual filter (a necessary step for the filter to be used in the real time context). As in the model of (3), the coefficients were estimated using the pseudo-inverse method. These additional terms can be interpreted in two ways: first, as a simple model of the visco-elastic properties of the musculoskeletal system, and second as a model of joint-related afferent feedback to the cortex. In either case, the intent was not to capture the full nonlinear and timing complexity of the system, but instead to explore the performance implications of having a small amount of additional information about the state of the arm in forming the predictive models.

## III. Results

Although the monkey was given a wide variety of target positions to attain, the shoulder and elbow joint torques were significantly correlated (average $R = 0.65$ over all data sets, $p < 10^{-20}$, Fisher's $R$ to $Z$ transform and $Z$ test [37]). This apparent synergy between the shoulder and elbow torques has been observed in human arm reaching as well [38], [39]. The mean peak correlation between the $X$ and $Y$ components of hand position was not substantial ($R = -0.04$). In addition, the highest magnitude correlation between hand position and torque was observed between $Y$ and the shoulder, but this correlation was not substantial ($R = -0.3$). The mean peak correlations between torque and angular velocity of the corresponding joint and between torque and angular acceleration were 0.34 and 0.61, respectively. Fig. 2 shows the power spectra of representative position and torque signals from data set RS2. Power in the position signals [Fig. 2(a), (b)] dropped dramatically from dc to $\sim$1 Hz. However, there was a significant peak within a band from 0.3–3 Hz in the torque signals [Fig. 2(c), (d)].

Using the linear filter decoder, we were able to reconstruct both the position and the joint torque signals. Fig. 3 shows examples of both from data set RS2 ($N = 86$ neurons). Fig. 3(a) and (b) shows the X and Y components of hand position. The corresponding shoulder and elbow torque predictions are shown in Fig. 3(c) and (d). The panels show the true value of the corresponding variable, the prediction of the variable, and the 95% confidence interval for the prediction (the computation of this interval is detailed in Appendix B). Although data were collected continuously, only successful trials were analyzed. Hence, the dashed lines indicate segments where discontinuous signals were concatenated for display purposes. The activity history of each neuron used in forming a prediction never crossed these discontinuities.

The higher frequency content of torque compared to position is evident in both the actual and the predicted signals. Prediction performance was assessed by computing the FVAF on test data that had not been used to build the model. In this example, the accuracy of torque prediction was comparable to that of hand position. However, across the entire 2.4 min of this test data set, FVAF values were 0.76 and 0.67 for shoulder and elbow torques, respectively, versus 0.83 and 0.80 for the X and Y hand positions, respectively.

Fig. 4 summarizes the average FVAF values (K = 20) across the six data sets. For individual experiments, FVAF ranged from 0.19 to 0.87 for joint torque, 0.34–0.86 for Cartesian position, and 0.36–0.88 for Cartesian velocity. Shoulder torque was predicted more accurately than elbow torque (mean FVAF difference= 0.107, paired bootstrap test, $p < 10^{-6}$). There was no significant difference between the predictions of $X$ and $Y$ position and velocity ($p < 0.68$ and $p < 0.17$, respectively, paired bootstrap test). Over the six data sets and 20 folds, the Cartesian position predictors outperformed the torque predictors by an average of 0.043 in the FVAF measure; this difference was significant according to a two-sample bootstrap test ($p < 0.002$). Cartesian velocity decoders performed on average better than both the Cartesian position and torque decoders by

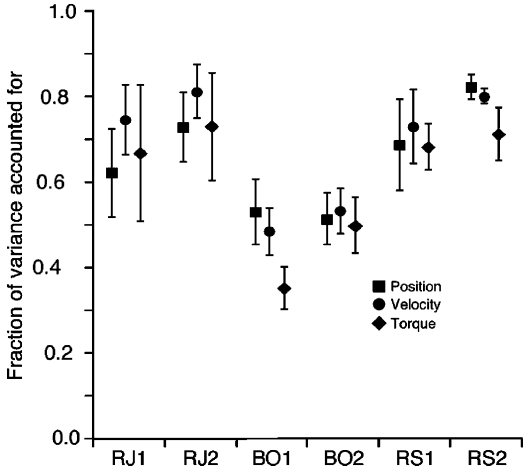


Fig. 4. Summary of decoding results. Mean FVAF by the decoding models, for Cartesian position (squares), Cartesian velocity (circles), and joint torque (diamonds). Markers indicate mean FAVF over 20 cross-validated folds. Error bars represent standard deviations over the 20 cross-validated folds.

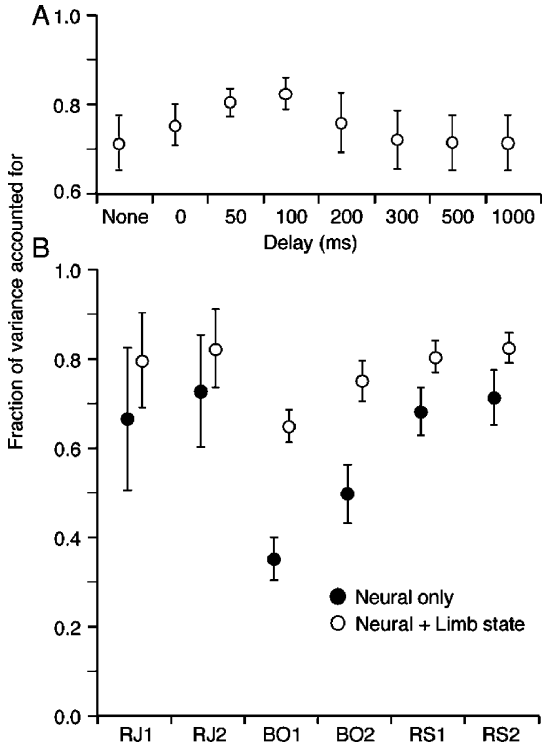


Fig. 5. Joint torque FVAF with the addition of simulated proprioceptive feedback. FVAF as a function of the time delay ($\Delta$) between spike discharge and feedback (including a no feedback condition) for data set RS2 (a). FVAF for all six data sets with (white) and without (black) feedback using the delay of $\Delta = 100$ ms (b).

0.033 and 0.077, respectively. These differences were significant according to a two-sample bootstrap test ($p < 0.01$ and $p < 10^{-6}$, respectively). The mean difference in FVAF values (over all six data sets) between training and test data was 0.03 and 0.04 for shoulder and elbow torque reconstructions, respectively, and 0.04 for both the $X$ and $Y$ components of the hand position; all differences were significant according to a paired bootstrap test ($p < 10^{-6}$). This indicates the possibility of a small over-fitting effect, though not a serious one.

### A. Proprioceptive Feedback and Torque Prediction

In the intact nervous system, accurate motor control depends on multiple sources of sensory feedback, including proprioception via both fast spinal reflexes and slower long-loop reflexes mediated through the cortex [40]. We simulated the effect of proprioceptive feedback by including inputs to the torque decoder [right side of Fig. 5(a) and (b)] that corresponded to the joint angular positions and velocities at a fixed time prior to the torque prediction. In order to ensure that the trained decoder was realizable in an online control context, the proprioceptive feedback was filtered using a causal Butterworth filter. This filter induced delays in these signals on the order of 50 ms. We assessed the performance of these modified decoders using the validation data sets by varying the feedback time lag ($\Delta$) from 0 to 1000 ms for data set RS2 [Fig. 5(a)]. Note that this feedback time lag is in addition to the delay induced by the filter. Decoding performance peaked at a delay of $\Delta = 100$ ms. For delays of 300 ms and greater, performance was comparable to having no proprioceptive feedback.

Over all six test data sets across the three animals, the torque decoding performance was significantly improved with the addition of proprioceptive feedback at a delay of $\Delta = 100$ ms [mean improvement was 0.168, $p < 10^{-6}$, paired bootstrap test; Fig. 5(b)].

### B. Temporal Structure of Decoders

As already discussed, the Cartesian position and joint torque signals have peak power at different frequencies. One question is whether these differences are reflected in the decoder coefficients. For a given filter lag, $i$, we computed the mean absolute filter coefficient, $\bar{f}_i$, across the set of neurons

$$\bar{f}_i = \frac{1}{N}\sum_{n=1}^{N} |f_i^n|. \tag{6}$$

This measure can be interpreted as the importance of time delay $i$ to the prediction made by the decoder, relative to the other time delays. Fig. 6 shows this measure as a function of delay for a representative experiment. Each curve corresponds to a single decoder type: Cartesian position, torque, and torque with proprioception. Because predictions by the different decoders are made in terms of different units, the absolute coefficient magnitude between decoders is arbitrary. The $\bar{f}_i$'s are therefore scaled so that the maximum for a given decoder is unity.

Fig. 6 shows that the Cartesian position decoder placed a majority of weight on cell activity in the first 450 ms, but also included substantial weight over the entire one second. In contrast, the torque decoders primarily incorporated information from the first 200–300 ms. This difference between the Cartesian position and torque decoders was consistent across the six data sets. This distinction may be due to the differences in the component frequencies contained within the two classes of predictions: because of its lower bandwidth, Cartesian position does not change as quickly, the decoder can average information from a longer history of neural signals. In contrast, the higher frequency content of the torque signals implies that only the recent history of

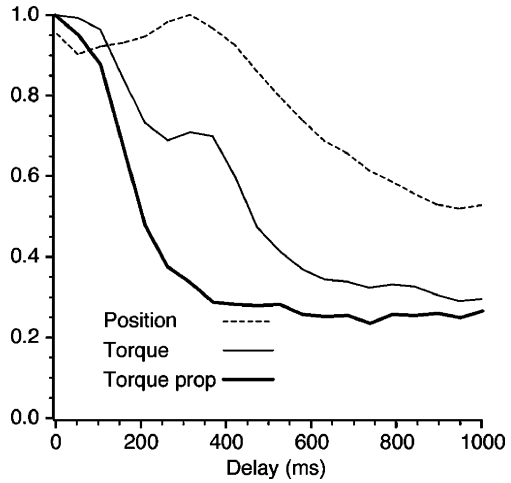


Fig. 6. Scaled mean absolute filter coefficient as a function of delay between filter time bin and arm state prediction. Each curve corresponds to a different decoder: Cartesian position (dashed line), torque (solid, thin), and torque with proprioception (solid, thick). Mean is computed over all cells from a single decoder.

the neural signals contains information relevant to the current prediction.

Fig. 6 also shows a distinction between the torque and the torque-with-proprioception decoders; this distinction was clear in half of the data sets. In particular, the torque decoder placed more emphasis on the 200-450 ms time range than did the modified decoder. As discussed above, substantial position information is present in the first 450 ms of neural data before movement. However, when joint position and velocity are explicitly available to the decoder from the feedback terms, the only information that must be extracted from the history of cell activity is the intended acceleration. Because the acceleration signals have peak power at higher frequencies than position, the decoder will focus on the information that is available just prior to the predicted movement.

### C. Stability of Learned Decoders

Ultimately, we are interested in the development of decoders for chronic use; one key question is the stability of a decoder over time. We examined this question by constructing a set of decoders using training data derived from the first half of an experimental session, and then comparing the performance on the trials from the third and fourth quarters of the session. As in the previous experiments, each of the six data sets was partitioned into 20 data folds, each containing equal numbers of trials. For each data set, the first ten folds were used to construct ten different decoders of Cartesian position and velocity and of torque (each model used nine of the ten available training folds). The performance of each decoder was tested using folds 11–15 (early) and 16–20 (late). The differences in performance for each of the three decoder types were not significant ($p < 0.09$, $p < 0.48$, and $p < 0.96$, respectively, according to a paired bootstrap test). This result suggests that the learned decoders are stable over the duration of the experimental session.

## IV. Discussion

We have shown that neural activity from ensembles of simultaneously recorded neurons in the primary motor cortex can be used to reconstruct time-varying joint torques at the shoulder and elbow during constrained movements of the arm in the horizontal plane. To our knowledge, this is the first demonstration of kinetic decoding of proximal arm movements. The accuracy of reconstructions of shoulder and elbow joint torque was nearly equivalent to that of Cartesian hand position and slightly less than that of Cartesian velocity. This study is intended as a demonstration of the feasibility of extracting kinetic information from MI for use in controlling a dynamic limb. Because of the significant remaining correlations between joint torque and movement kinematics, it is impossible to make strong assertions about whether either set of signals represents the fundamental signals "encoded" by MI. Nonetheless, it is quite possible that a BMI-controlled prosthetic device that would both move and exert contact force, would benefit from the use of kinetic control signals, either alone or in combination with kinematic signals.

### A. Proprioceptive Feedback

We have also demonstrated that the addition of limb-state information to the torque decoder resulted in significant improvements in decoding accuracy. The joint position and velocity were filtered using a causal filter, which induces a signal delay but affords a real-time implementation. These very simple simulations of linear proprioceptive feedback suggest that a practical BMI for use in spinal injured patients would benefit from the introduction of artificial sensory signals to the controller that include the state of the controlled device. It should be emphasized that the sensory signals we simulated were fed back to the decoder and not to the animal.

The modified torque decoder performed substantially better than both the position and velocity decoders. However, it is important to note that this is not an entirely fair comparison to make as the latter decoders do not benefit from the delayed proprioceptive information. One could certainly design a comparable approach for these decoders (e.g., providing torque as an input to these decoders). However, such an approach would not be applicable to an online control context.

The randomly-placed targets used in this study allowed movements to be significantly less constrained than are the movements to a limited number of fixed targets. However, there remained significant linear correlations between joint angular position/velocity and torque. If these signals were further decoupled, the benefit of this simple linear feedback would certainly be reduced. Incorporation of nonlinear feedback signals should also be considered.

### B. Technical Issues and Potential Improvements

In our analysis, we have followed Serruya *et al.* [29] in using a "fraction of variance accounted for" measure of performance as opposed to the Coefficient of Determination. FVAF is stricter in that it requires a perfect match between the prediction and the observation, rather than a simple correlation. This distinction is particularly important once one begins to use these predictions to drive the motion of a prosthetic or robotic arm. Furthermore, the computation of the Coefficient of Determination statistic involves a linear regression step that makes use of the test data set to select optimal gain and offset parameters. Because the

training data are being used in the selection of model parameters, the data set is not independent of the training process. Hence, a significant bias can be introduced into the evaluation process that can mask the utility of the resulting predictors in novel/independent contexts, such as when controlling a prosthetic arm.

In practice, the pseudo-inverse solution to this form of linear filter decoder can be unstable when training set sizes are small and/or the number of recorded cells is large. We are exploring the use of a modified form of the pseudo-inverse method that includes a smoothness term in the error function. This method addresses the function over-fitting issues that can arise in these unstable situations, leading in some cases to dramatic improvements in performance.

### C. Relation Between Kinematic and Kinetic Parameters

At first glance, it is perhaps not surprising that the accuracy of joint torque reconstruction is similar to that of hand position and velocity, given their relationship through the equations of motion and arm kinematics. However, it should be emphasized that joint torque represents a much richer signal, as is evident from its significantly larger bandwidth. Therefore, it is not obvious *a priori* that the torque decoding performance would have been comparable to that of hand position. It is possible that the slightly higher frequency content of the elbow torque signals may have been a factor in the lower prediction quality of elbow torque compared to that of the shoulder. Because of the strong correlations between joint torque and both angular velocity and acceleration, we cannot address the long-standing controversy as to whether MI codes primarily for kinetic versus kinematic parameters of movement. However, our primary aim in this study was to determine whether kinetic decoding is possible for BMI applications, comparable to results from previous studies that have decoded position and velocity.

Our results are consistent with the observations of other groups that have studied single neurons and found significant correlations with both kinetic as well as kinematic signals [6], [41]–[43]. There is some evidence that the most caudal area of MI within the bank of the central sulcus may be more be directly related to muscle activity and the dynamics of movement, as compared to the precentral gyrus where our recordings were made [44]. Therefore, torque decoding may be even more accurate if it could be based on motor cortical populations within the bank of the central sulcus.

### D. Implications for BMI Development

It would be of great interest to determine a monkey's ability to use kinetic signals for real-time, closed-loop control. Such a control system might provide greater ability to generalize control across a variety of dynamical conditions and external loading. One potential concern with kinetic control is that small torque prediction errors, when applied open loop to a forward dynamics limb model will lead to significant position error. Our analyses suggest that it takes at least 400 ms for a substantial error to accumulate. This degree of drift is unlikely to be problematic in the closed-loop context, as the subject could correct for any significant position error via visual feedback. This situation is not unlike the significant improvement that was realized for position control when the brain-control loop was first closed. Initial estimates (based on open-loop studies) of the number of neurons that would be required to achieve adequate control ranged into the hundreds of neurons [14]. However, when monkey subjects were given the ability to correct position decoding errors, control was achieved with only tens of neurons [15], [16].

## Appendix A
## Determination of Parameter Values

Definitions and values of quantities used in (1) and (2) are given in Table II. Note that only inter-joint lengths ($L_1$ and $L_3$) appear directly in (1) and (2), because they contribute to the effective inertia components for segments 2 and 4, respectively. $L_2$ and $L_4$ thus do not directly enter the equations, although $L_2$ is employed in the kinematics equations relating Cartesian position of the KINARM handle to angular coordinates.

Rotational inertias for all components of the monkey/KINARM system were computed with respect to their proximal pivots, by the addition of products of their masses with squared distances between pivots and centers of mass of each component. In computing inertias of animal and KINARM segments, the hand was treated as a point mass at the location of the palm, and forearm troughs and rests were treated as linear masses located at their centers. The upper arm was treated as a uniform on-axis cylinder.

## Appendix B
## Computation of Prediction Interval

The prediction interval is computed as follows. Define $R_j$ as the column vector at time index $j$ that encodes the activity of $L$ neurons at the $N$ time bins preceding $j$

$$R_j = \left[r^1_{j-1},\, r^1_{j-2},\, r^1_{j-3},\, \ldots,\, r^1_{j-L},\, r^2_{j-1}, \ldots,\, r^N_{j-L},\, 1\right]^T.$$

Define $R$ to be the matrix containing all $M$ of the $R_j$ vectors within the training data set

$$R = [R_1,\, R_2,\, R_3,\, \ldots,\, R_M].$$

Then, the prediction interval at some arbitrary time index $j$ (whether it is in the training or testing data set) is

$$\hat{p_j} \pm \sigma\ t_{1-\alpha/2,\, M-L\times N}\sqrt{1 + {R_j}^T(R^TR)^{-1}R_j}$$

where $\sigma$ is the standard deviation of the variable being predicted (measured with respect to the training set), and $t_{1-\alpha/2,\, M-L\times N}$ is the $1-\alpha/2$ quantile of the $t$-distribution with $M - L \times N$ degrees of freedom.

## Acknowledgment

The authors would like to thank M. Fellows, E. Gunderson, Z. Haga, D. Paulsen, and J. Reimer for their help with the surgical implantation of the arrays, training of monkeys, and data collection. Inertial properties of segments of the KINARM

were supplied by I. Brown. The authors also thank D. Goldberg for his assistance in conducting and analyzing the decoding experiments.

## REFERENCES


[1] E. V. Evarts, "Relation of pyramidal tract activity to force exerted during voluntary movement," *J. Neurophysiol.*, vol. 31, pp. 14–27, 1968.

[2] A. P. Georgopoulos, J. F. Kalaska, R. Caminiti, and J. T. Massey, *On the Relations Between the Direction of Two-Dimensional Arm Movements and Cell Discharge in Primate Motor Cortex*, vol. 2, pp. 1527–1537, 1982.

[3] A. M. Smith, M. C. Hepp-Reymond, and U. R. Wyss, "Relation of activity in precentral cortical neurons to force and rate of force change during isometric contractions of finger muscles," *Exp. Brain Res.*, vol. 23, pp. 315–32, 1975.

[4] M.-C. Hepp-Reymond, U. R. Wyss, and R. Anner, *Neuronal Coding of Static Force in the Primate Motor Cortex*, vol. 74, pp. 287–291, 1978.

[5] P. D. Cheney and E. E. Fetz, "Functional classes of primate corticomotoneuronal cells and their relation to active force," *J. Neurophysiol.*, vol. 44, pp. 773–91, 1980.

[6] J. F. Kalaska, D. A. D. Cohen, M. L. Hyde, and M. Prud'homme, *A Comparison of Movement Direction-Related Versus Load Direction-Related Activity in Primate Motor Cortex, Using a Two-Dimensional Reaching Task*, vol. 9, pp. 2080–2102, 1989.

[7] M. Taira, J. Boline, N. Smyrnis, A. P. Georgopoulos, and J. Ashe, "On the relations between single cell activity in the motor cortex and the direction and magnitude of three-dimensional static isometric force," *Exp. Brain Res.*, vol. 109, pp. 367–76, 1996.

[8] D. W. Cabel, P. Cisek, and S. H. Scott, "Neural activity in primary motor cortex related to mechanical loads applied to the shoulder and elbow during a postural task," *J. Neurophysiol.*, vol. 86, pp. 2102–8, 2001.

[9] L. E. Sergio, C. Hamel-Paquet, and J. F. Kalaska, "Motor cortex neural correlates of output kinematics and kinetics during isometric-force and arm-reaching tasks," *J. Neurophysiol.*, vol. 94, pp. 2353–78, 2005.

[10] A. P. Georgopoulos, R. Caminiti, and J. F. Kalaska, "Static spatial effects in motor cortex and area 5: Quantitative relations in a two-dimensional space," *Exp. Brain Res.*, vol. 54, pp. 446–454, 1984.

[11] L. Paninski, M. R. Fellows, N. G. Hatsopoulos, and J. P. Donoghue, "Spatiotemporal tuning of motor cortical neurons for hand position and velocity," *J. Neurophysiol.*, vol. 91, pp. 515–532, 2004.

[12] D. W. Moran and A. B. Schwartz, "Motor cortical representation of speed and direction during reaching," *J. Neurophysiol.*, vol. 82, pp. 2676–92, 1999.

[13] D. W. Moran and A. B. Schwartz, "Motor cortical activity during drawing movements: Population representation during spiral tracing," *J. Neurophysiol.*, vol. 82, pp. 2693–704, 1999.

[14] J. Wessberg, C. R. Stambaugh, J. D. Kralik, P. D. Beck, M. Laubach, J. K. Chapin, J. Kim, S. J. Biggs, M. A. Srinivasan, and M. A. Nicolelis, "Real-time prediction of hand trajectory by ensembles of cortical neurons in primates," *Nature*, vol. 408, pp. 361–5, 2000.

[15] M. D. Serruya, N. G. Hatsopoulos, L. Paninski, M. R. Fellows, and J. P. Donoghue, "Instant neural control of a movement signal," *Nature*, vol. 416, pp. 141–2, 2002.

[16] D. M. Taylor, S. I. Tillery, and A. B. Schwartz, "Direct cortical control of 3D neuroprosthetic devices," *Science*, vol. 296, pp. 1829–32, 2002.

[17] J. R. Wolpaw and D. J. McFarland, "Control of a two-dimensional movement signal by a noninvasive brain-computer interface in humans," in *Proc. Nat. Acad. Sci.*, 2004, vol. 101, pp. 17849–54.

[18] D. R. Humphrey, E. M. Schmidt, and W. D. Thompson, "Predicting measures of motor performance from multiple cortical spike trains," *Science*, vol. 170, pp. 758–62, 1970.

[19] J. M. Carmena, M. A. Lebedev, R. E. Crist, J. E. O'Doherty, D. M. Santucci, D. F. Dimitrov, P. G. Patil, C. S. Henriquez, and M. A. Nicolelis, "Learning to control a brain-machine interface for reaching and grasping by primates," *Public Library Sci., Biol.*, vol. 1, pp. 1–16, 2003.

[20] M. M. Morrow and L. E. Miller, "Prediction of muscle activity by populations of sequentially recorded primary motor cortex neurons," *J. Neurophysiol.*, vol. 89, pp. 2279–88, 2003.

[21] D. M. Santucci, J. D. Kralik, M. A. Lebedev, and M. A. Nicolelis, "Frontal and parietal cortical ensembles predict single-trial muscle activity during reaching movements in primates," *Eur. J. Neurosci.*, vol. 22, pp. 1529–40, 2005.

[22] D. T. Westwick, E. A. Pohlmeyer, S. A. Solla, L. E. Miller, and E. J. Perreault, "Identification of multiple-input systems with highly coupled inputs: Application to EMG prediction from multiple intracortical electrodes," *Neural Comput.*, vol. 18, pp. 329–55, 2006.

[23] E. A. Pohlmeyer, S. A. Solla, E. J. Perreault, and L. E. Miller, "Prediction of upper limb muscle activity from motor cortical discharge during reaching," *.J Neural Eng.*, vol. 4, pp. 369–79, 2007.

[24] S. H. Scott, "Apparatus for measuring and perturbing shoulder and elbow joint positions and torques during reaching," *J. Neurosci. Methods*, vol. 89, pp. 119–27, 1999.

[25] J. M. Hollerbach and T. Flash, "Dynamic interactions between limb segments during planar arm movement," *Biol. Cyberkinetics*, vol. 44, pp. 67–77, 1982.

[26] E. J. Cheng and S. H. Scott, "Morphometry of macaca mulatta forelimb. I. Shoulder and elbow muscles and segment inertial parameters," *J. Morphol.*, vol. 245, pp. 206–224, 2000.

[27] H. Goldstein, *Classical Mechanics*. Reading, MA: Addison-Wesley, 1959.

[28] A. V. Oppenheim and R. W. Shafer, *Discrete-Time Signal Processing*. Englewood Cliffs, NJ: Prentice-Hall, 1989.

[29] M. Serruya, N. Hatsopoulos, M. Fellows, L. Paninski, and J. Donoghue, "Robustness of neuroprosthetic decoding algorithms," *Biol. Cybern.*, vol. 88, pp. 219–28, 2003.

[30] N. Hatsopoulos, J. Joshi, and J. O'Leary, "Decoding continuous and discrete motor behaviors using motor and premotor cortical ensembles," *J. Neurophysiol.*, vol. 92, pp. 1165–1174, 2004.

[31] R. Penrose, "A generalized inverse for matrices," in *Proc. Cambridge Philos. Soc.*, 1955, vol. 51, pp. 406–413.

[32] B. S. Everitt, *Cambridge Dictionary of Statistics*, 2nd ed. Cambridge, U.K.: Cambridge Univ. Press, 2002.

[33] M. Stone, "Cross-validatory choice and assessment of statistical predictions," *J. R. Stat. Soc. Series B-Methodological*, vol. 36, pp. 111–147, 1974.

[34] C. Bishop, *Neural Networks for Pattern Recognition*. Oxford, U.K.: Oxford Univ. Press, 1996.

[35] M. W. Browne, "Cross-validation methods," *J. Math. Psychol.*, vol. 44, pp. 108–132, 2000.

[36] S. S. Shapiro and M. B. Wilk, "An analysis of variance test for normality (complete samples)," *Biometrika*, vol. 52, pp. 591–611, 1965.

[37] P. R. Cohen, *Empirical Methods for Computer Science*. Cambridge, MA: MIT Press, 1995.

[38] G. L. Gottlieb, Q. Song, D. A. Hong, G. L. Almeida, and D. Corcos, "Coordinating movement at two joints: A principle of linear covariance," *J. Neurophysiol.*, vol. 75, pp. 1760–4, 1996.

[39] G. L. Gottlieb, Q. Song, D. A. Hong, and D. M. Corcos, "Coordinating two degrees of freedom during human arm movement: Load and speed invariance of relative joint torques," *J. Neurophysiol.*, vol. 76, pp. 3196–206, 1996.

[40] P. D. Cheney and E. E. Fetz, "Corticomotoneuronal cells contribute to long-latency stretch reflexes in the rhesus monkey," *J. Physiol.*, vol. 349, pp. 249–72, 1984.

[41] W. T. Thach, "Correlation of neural discharge with pattern and force of muscular activity, joint position, and direction of intended next movement in motor cortex and cerebellum," *J. Neurophysiol.*, vol. 41, pp. 654–676, 1978.

[42] S. Kakei, D. S. Hoffman, and P. L. Strick, "Muscle and movement representations in the primary motor cortex," *Science*, vol. 285, pp. 2136–2139, 1999.

[43] S. Kakei, D. S. Hoffman, and P. L. Strick, "Direction of action is represented in the ventral premotor cortex," *Nat. Neurosci.*, vol. 4, pp. 1020–5, 2001.

[44] J. A. Rathelot and P. L. Strick, "Muscle representation in the macaque motor cortex: An anatomical perspective," in *Proc. Nat. Acad. Sci.*, 2006, vol. 103, pp. 8257–62.


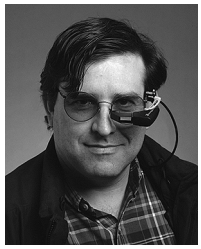

**Andrew H. Fagg** (M'97) received the B.S. degree in applied mathematics/computer science from Carnegie-Mellon University, Pittsburgh, PA, in 1989, and the M.S. and Ph.D. degrees in computer science from the University of Southern California, Los Angeles, in 1991 and 1996, respectively.

He is currently an Associate Professor of Computer Science at the University of Oklahoma, Norman. His research focuses on the computational issues surrounding the symbiotic relationships between primates and machines.

**Greg Ojakangas** received the B.S. degree in physics and geology from the University of Minnesota, Duluth, in 1982, the M.S. degree in geophysics in 1985, and the Ph.D. degree in planetary science from the California Institute of Technology, Pasadena, in 1988.

He is currently an Associate Professor of Physics at Drury University, Springfield, MO, and a consultant for NASA in orbital debris studies. His primary research has been in planetary astrophysics, but recently he has turned his attention, in part, to computational neuroscience and robotic arms actuated by simulated muscles.

**Lee E. Miller** received the B.A. degree in physics from Goshen College, Goshen, IN, in 1980, and the M.S. degree in biomedical engineering and the Ph.D. degree in physiology from Northwestern University, Evanston, IL, in 1983 and 1989, respectively. He completed two years of postdoctoral training in the Department of Medical Physics, University of Nijmegen, The Netherlands.

He is currently a Professor in the Departments of Physiology, Physical Medicine and Rehabilitation, and Biomedical Engineering at Northwestern University. His primary research interests are in the cortical control of muscle activity and limb movement, and in the development of brain–machine interfaces that attempt to mimic normal physiological systems.

**Nicholas G. Hatsopoulos** received the B.A. degree in physics from Williams College, Williamstown, MA, in 1984, the M.S. degree in psychology in 1991 and the Ph.D. degree in cognitive science from Brown University, Providence, RI, in 1992.

He joined the faculty at the University of Chicago in 2002 and is currently an Associate Professor in the Department of Organismal Biology and Anatomy and is Chairman of the Committee on Computational Neuroscience. His research focuses on the neural coding of motor behavior in large cortical ensembles and on the development of brain–machine interfaces.